Applied Catalysis B: Environmental 138–139 (2013) 253–259

Contents lists available at SciVerse ScienceDirect

Applied Catalysis B: Environmental

journal homepage: www.elsevier.com/locate/apcatb

Catalytic removal of benzene over CeO_2–MnO_x composite oxides prepared by hydrothermal method

Zhen Wang[a], Genli Shen[b,c], Jiaqi Li[b,c], Haidi Liu[b], Qi Wang[a,*], Yunfa Chen[b,*]

[a] CAS Key Laboratory of Standardization and Measurement for Nanotechnology, National Center for Nanoscience and Technology, Beijing 100190, China
[b] State Key Laboratory of Multiphase Complex Systems, Institute of Process Engineering, Chinese Academy of Sciences, Beijing 100190, China
[c] Graduate University of Chinese Academy of Sciences, Beijing 100049, China

ARTICLE INFO

Article history:
Received 20 November 2012
Received in revised form 12 January 2013
Accepted 5 February 2013
Available online 24 February 2013

Keywords:
CeO_2–MnO_x composite oxides
Oxygen vacancy
Synergistic effect
Benzene oxidation

ABSTRACT

A series of CeO_2–MnO_x composite oxides were synthesized through hydrothermal method and the complete catalytic oxidation of benzene were examined. The effects of the Ce_{at}/Mn_{at} atomic ratio on the features of catalyst structure and catalytic behavior were researched. The results exhibited that the catalytic properties of CeO_2–MnO_x composite oxides were higher than pure CeO_2 or MnO_x. When the Ce_{at}/Mn_{at} ratio was 3:7, the catalytic activity reached the best. By means of testing, the data revealed that the synergistic effects existed in the composite oxides, which resulted in the enhancement of catalytic abilities. In the main phase, MnO_x provided available oxygen species and CeO_2 enhanced oxygen mobility. In addition, the nature of oxygen vacancy of catalysts was also studied through positron annihilation spectrum. The results showed that the concentration of oxygen vacancy for CeO_2–MnO_x composite oxides changed comparing with pure CeO_2 or MnO_x, which also caused the activity differences over benzene.

© 2013 Elsevier B.V. All rights reserved.

1. Introduction

Volatile organic compounds (VOCs) produced by industrial manufacturing are an important class of air pollutants. Many environmental problems, such as offensive odors, toxic emissions, ozone formation and petrochemical smog are related to the emissions of VOCs. The reduction of the emissions of VOCs is a very important environmental issue for human health. At present, VOCs are usually removed by thermal oxidation, catalytic oxidation, adsorption and absorption [1]. Among these techniques, catalytic oxidation is regarded as an effective way for VOCs emission control, due to higher destructive efficiency than adsorption, and lower operating temperature and harm reaction by-products than thermal oxidation [2–5]. In addition, catalytic oxidation does not require additional fuel, reducing energy consumption and avoiding the formation of thermal NO_x.

Benzene is a hazardous volatile organic compound presenting in various industries such as chemical, petrochemical, paint and coating and steel manufacture. Catalytic oxidation is regarded as one of the most promising routes for the effective removal of benzene. Supported noble metal catalysts, typically Pd, have been generally preferred for the complete oxidation of benzene due to the higher activity [1,6–9]. However, the usage of these noble metals is limited due to high cost, low thermal stability and sensitivity to poisoning. Transition metal oxide-based catalysts are suitable alternative because of higher thermal stability and lower price [10]. In certain cases, transition metal oxides can be actually more active than noble metal catalysts [11].

Perovskites, zirconia-based catalysts, manganese and cobalt oxides have been claimed for their effectiveness in VOCs oxidation, among which, manganese oxides are the most active oxide catalysts in VOC oxidation [11–14]. Ceria (CeO_2), as a rare earth oxide, has been extensively investigated in heterogeneous catalysis due to its high oxygen storage capacity. More recently, CeO_2-based mixed oxides have also been employed for VOCs removal [15–17]. CeO_2–MnO_x mixed oxides can be applied as heterogeneous catalysts for the abatement of contaminants in the liquid and gas phases, such as the catalytic reduction of NO and oxidation of acrylic acid and formaldehyde [18–21], which exhibit much higher catalytic activity than those of pure MnO_x and CeO_2.

In this article, we investigate the catalytic behavior of CeO_2–MnO_x composite oxide catalysts prepared via the hydrothermal method through the complete catalytic oxidation of benzene. Their catalytic activities differences are analyzed in detail for different Mn/Ce atomic ratio oxides. The purpose of this study is to discuss the roles of crystal vacancy produced by the formation of solid solution and interaction between CeO_2 and MnO_x in the combustion of benzene.

* Corresponding authors. Tel.: +86 10 82545755; fax: +86 10 62525716.
E-mail addresses: wangq@nanoctr.cn (Q. Wang), yfchen@home.ipe.ac.cn (Y. Chen).

0926-3373/$ – see front matter © 2013 Elsevier B.V. All rights reserved.
http://dx.doi.org/10.1016/j.apcatb.2013.02.030

2. Experimental

2.1. The preparation of CeO_2–MnO_x composite oxides

The chemicals used in this work, including $Ce(NO_3)_3{\cdot}6H_2O$ (99%), $Mn(NO_3)_2$ solution (50%), NaOH (98%), and ethanol, were purchased from Beijing Chemicals Company (Beijing, China). CeO_2–MnO_x composite oxides with different Mn/Ce atomic ratio (Mn/Ce ranging from 1:9 to 9:1) were synthesized by a hydrothermal process. Briefly, $Ce(NO_3)_3{\cdot}6H_2O$ and $Mn(NO_3)_2$ in appreciate amounts were dissolved in a 10 mL H_2O and mixed with a 6 M NaOH solution. The solution was then transferred to an autoclave (100 mL) and gradually heated to 120 °C, then kept at the given temperature for 24 h. The precipitates in autoclaves were collected by centrifugation, washed with distilled water and ethanol several times. The obtained materials, labeled as Ce_xMn_{1-x} (where x refers to the Ce/(Ce + Mn) atomic ratio) were dried at 80 °C overnight and calcined at 550 °C for 4 h. Pure CeO_2 and MnO_x were also prepared using the similar process as reference.

2.2. Characterization technique

The crystal phase of the materials was characterized on X-ray diffraction (XRD, Philips X'pert PRO) equipped with a Cu Kα radiation source (λ = 0.154187 nm) at a scanning rate of 0.03°/s (2θ from 10° to 90°). The assignment of the crystalline phases was based on the ICSD data base (Mn_2O_3 no. 89-4836; CeO_2 no. 81-0792). The inductively Coupled Plasma (ICP) was tested to measure the contents of Ce and Mn ions. The morphology and structure of samples were observed using transmission electron microscopy (TEM) (JEOL JEM-2010F) with an accelerating voltage of 200 kV.

The BET specific surface area (S_{BET}) was measured by physical adsorption of N_2 at the liquid nitrogen temperature using an Autosorb-1 analyzer (Quantachrome). Before measurement, the samples were degassed at 300 °C for 4 h under vacuum. Surface composition was determined by X-ray photoelectron spectroscopy (XPS) using an ESCALab220i-XL electron spectrometer from VG Scientific with a monochromatic Al Kα radiation. The binding energy (BE) was referenced to the C1s line at 284.8 eV from adventitious carbon. Positron annihilation spectrum was tested in order to research the nature of oxygen vacancy in the catalysts.

Hydrogen temperature-programmed reduction (H_2-TPR) was performed with a U-type quartz reactor equipped with Automated Catalyst Characterization System (Autochem 2920, MICROMERITICS). A 50 mg sample (40–60 mesh) was loaded and pretreated with a 5% O_2 and 95% He mixture (30 mL/min) at 150 °C for 1 h and cooled to 50 °C under He flow. The samples were then heated to 900 °C at a rate of 10 °C/min under the flow of a 10% H_2 and 90% Ar mixture (30 mL/min).

2.3. Catalytic activity tests

Activity tests for catalytic oxidation of benzene over Ce_xMn_{1-x} composite catalysts were performed in a continuous-flow fixed-bed reactor under atmospheric pressure, containing 100 mg of catalyst samples (40–60 mesh). A standard reaction gas containing 1000 ppm benzene and 20% O_2 in N_2 was fed with a total flow rate of 100 mL/min. The weight hourly space velocity (WHSV) was typically 60,000 mL g^{-1} h^{-1}. The reactants and the products were analyzed on-line using a GC/MS (Hewlett-Packard 6890N gas chromatograph interfaced to a Hewlett-Packard 5973 N mass selective detector) with a HP-5MS capillary column (30 m × 0.25 mm × 0.25 μm) and another GC (GC112A, Shangfen, China) with a carbon molecule sieve column. The conversion of benzene ($X_{benzene}$, %) was calculated as follows:

$$X_{benzene} = \frac{C_{benzene(in)} - C_{benzene(out)}}{C_{benzene(in)}} \times 100\% \quad (1)$$

where $C_{benzene\ (in)}$ (ppm) and $C_{benzene\ (out)}$ (ppm) are the concentrations of benzene in the inlet and outlet gas, respectively.

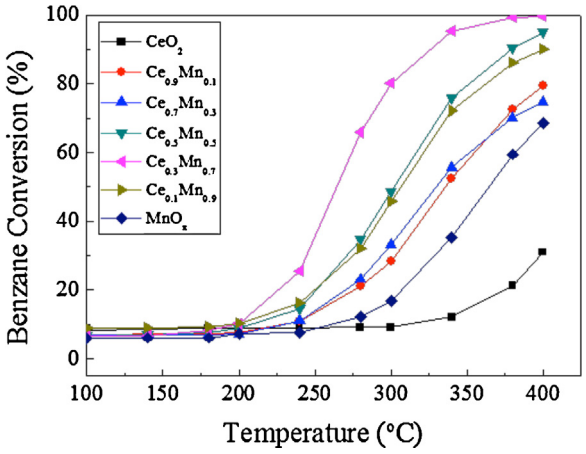

Fig. 1. C_6H_6 conversion (%) over CeO_2, MnO_x and Ce_xMn_{1-x} catalysts as a function of reaction temperature (°C).

3. Results and discussion

3.1. Catalytic oxidation activity of Ce_xMn_{1-x} composite oxides for benzene

The catalytic performances of CeO_2, MnO_x and Ce_xMn_{1-x} catalysts were evaluated in the oxidation of benzene. The catalytic conversion of benzene as a function of the temperature, 100–400 °C, is shown in Fig. 1. It can be acquired that the least active catalyst is CeO_2 followed by MnO_x. Upon addition of Mn to CeO_2, the activity increases monotonically up to a Mn content of 70 at.% and $Ce_{0.3}Mn_{0.7}$ is the most active among all catalysts achieving complete benzene conversion at ca.375 °C. When the Mn content continuously increases to 90 at.%, $Ce_{0.1}Mn_{0.9}$, the catalytic activity starts to decrease, even worse than that of $Ce_{0.5}Mn_{0.5}$, which indicates that the optimum ratio (Ce/Mn) is 3:7 for Ce_xMn_{1-x} catalysts to reach the best benzene conversion. In addition, the MnO_x and CeO_2 catalysts achieve full conversion above 600 °C. They both exhibit the negative activity over benzene comparing with that of Ce_xMn_{1-x}, which is probably related with the formation of the solid solution and the existence of synergistic effect between components for Ce_xMn_{1-x} composite oxides. This illustration will be researched in the following text.

3.2. Characterization of Ce_xMn_{1-x} catalysts

Fig. 2a shows the XRD patterns of the samples in the angular range 20°–70° 2θ. For pure MnO_x, the intensive and sharp diffractions at 2θ = 23.1°, 32.9°, 38.2°, 45.3°, 49.4°, 55.2° and 65.8° could be primarily attributed to Mn_2O_3 (PDF# 89-4836/65-1798). The diffraction peaks at 2θ = 28.5°, 33.0°, 47.4°, 56.4° and 59.2° in the XRD profile of the pure cerium oxide clearly demonstrate the presence of cubic fluorite structure of CeO_2 (PDF# 81-0792). However, the XRD patterns of the Ce_xMn_{1-x} mixed oxide ($x \geq 0.5$) do not show any diffraction of manganese oxides, and only broad reflections due to CeO_2 are observed. This is in good consistent with recent observations that the phase composition of Ce_xMn_{1-x} oxides strongly depended on the molar ratios of manganese and cerium oxides

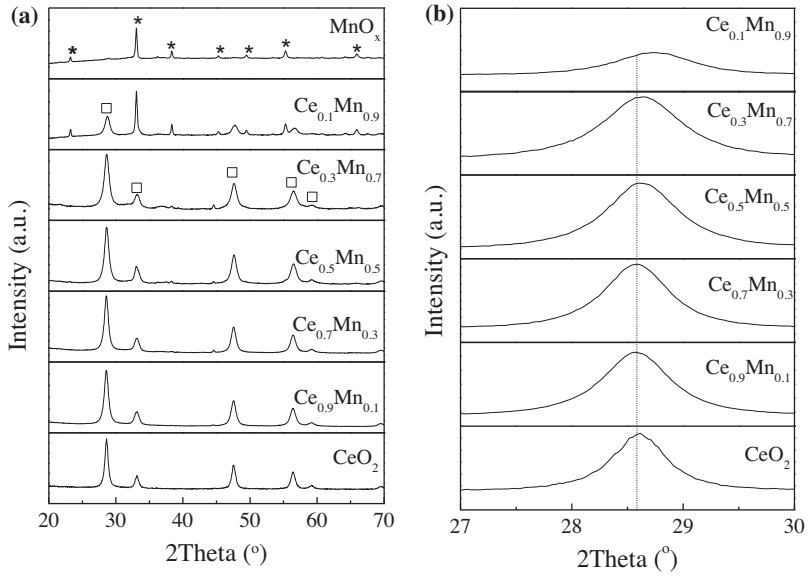

Fig. 2. XRD patterns of CeO_2–MnO_x composite oxides: (a) wild angle patterns, and (b) enlarged-zone patterns. Crystalline phases detected: (*), Mn_2O_3 and (□), CeO_2.

[22]. The diffraction patterns of Ce_xMn_{1-x} mixed oxides at $x \leq 0.3$ show crystallization of Mn_2O_3, whereas those at $x \geq 0.5$ consist of only broad peaks attributed to CeO_2 due to the formation of solid solution between Mn_2O_3 and CeO_2. For the Ce_xMn_{1-x} oxide system ($x \geq 0.5$), the solid solution is highly possible to be formed during the precipitation and calcination processes. This can be further evidenced by the fact that the diffraction peaks of CeO_2 in the composite oxides are slightly shifted to higher values of the Bragg angles, compared with the pure CeO_2 (Fig. 3b). Since the ionic radius of Mn^{3+} (0.066 nm) is smaller than that of the Ce^{4+} (0.1098 nm), the incorporation of Mn^{3+} into the CeO_2 lattice to form CeO_2–MnO_x solid solution would result in remarkable decrease in the lattice parameter of CeO_2 in the Ce_xMn_{1-x} mixed oxide. Therefore, the diffraction peaks of CeO_2 are slightly shifted to higher values. The lattice constants of all the Ce_xMn_{1-x} have been calculated according to the XRD data, as shown in Supporting Information.

The morphology and structure of samples were characterized by TEM. Fig. 3a shows the HRTEM image of pure CeO_2. It is seen that CeO_2 exhibits the rod-like morphology. When viewed along the [1 1 0] direction, the lattice spacing of the fringes perpendicular to the elongation direction of the nanorod is 0.19 nm, showing that the CeO_2 nanorods prefer to expose the (1 1 0) plane. Fig. 3b shows the HRTEM image of $Ce_{0.3}Mn_{0.7}$. Through the picture, it can be acquired that the morphology of sample has changed. CeO_2 nanorod has distinguished instead of nanoparticle and pure Mn_2O_3 can also be observed. They both expose their each stable plane (1 1 1) and (2 2 2), respectively. Meanwhile, it is worthy to note that the grain boundary between CeO_2 and Mn_2O_3 has no dislocation as shown in red circle, which indicates that they can achieve mutual solubility to form interaction. Fig. 3c exhibits the HRTEM image of pure Mn_2O_3. Through measuring the lattice spacing of the fringe, Mn_2O_3 is mainly enclosed by (2 2 2) plane.

The oxidation state of catalyst surface species was examined by XPS analysis. Fig. 4a presents the XPS spectra of the Ce3d core levels for all samples. Six peaks labeled as V_0 (882.3 eV), V_1 (888.6 eV), V_2 (897.7 eV), V_0' (900.6 eV), V_1' (906.9 eV) and V_2' (916.1 eV) refer to three pairs of spin–orbit doublets, which can be identified as characteristic of Ce^{4+} 3d final states [23,24]. The high BE doublet (V_2/V_2') is attributed to the final state of Ce(IV)$3d^94f^0O2p^6$, doublet (V_1/V_1') is originated from the state of Ce(IV)$3d^94f^1O2p^5$, and doublet V_0/V_0' corresponds to the state of Ce(IV)$3d^94f^2O2p^4$. These peaks strongly suggest that the oxidation state of Ce for all samples is predominantly tetravalent [25] and the presence of manganese ions does not affect the oxidation state of cerium [26]. In addition, the character peaks of Ce^{3+} are also observed from the doublet U_1/U_1' at 885.7 and 903.5 eV, which are characteristic of Ce^{3+} 3d final states (Ce(III)$3d^94f^2O2p^5$).

Fig. 4b shows the Mn 2p XPS spectra of Ce_xMn_{1-x} mixed oxides, in which Mn 2p doublet can be distinguished. The binding energies of the Mn $2p_{3/2}$ component appear at 641.6 eV and those for Mn $2p_{1/2}$ appear at 653.3 eV. The spin orbit splitting is $\Delta E = 11.7$ eV and the width is 3.62 eV. According to literature data [22], the observed

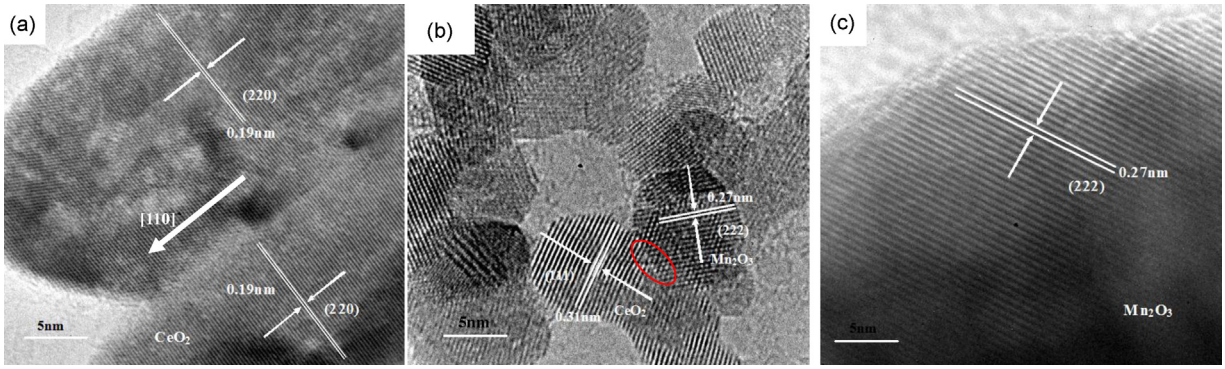

Fig. 3. The TEM images of CeO_2 (a), $Ce_{0.3}Mn_{0.7}$ (b) and Mn_2O_3 (c).

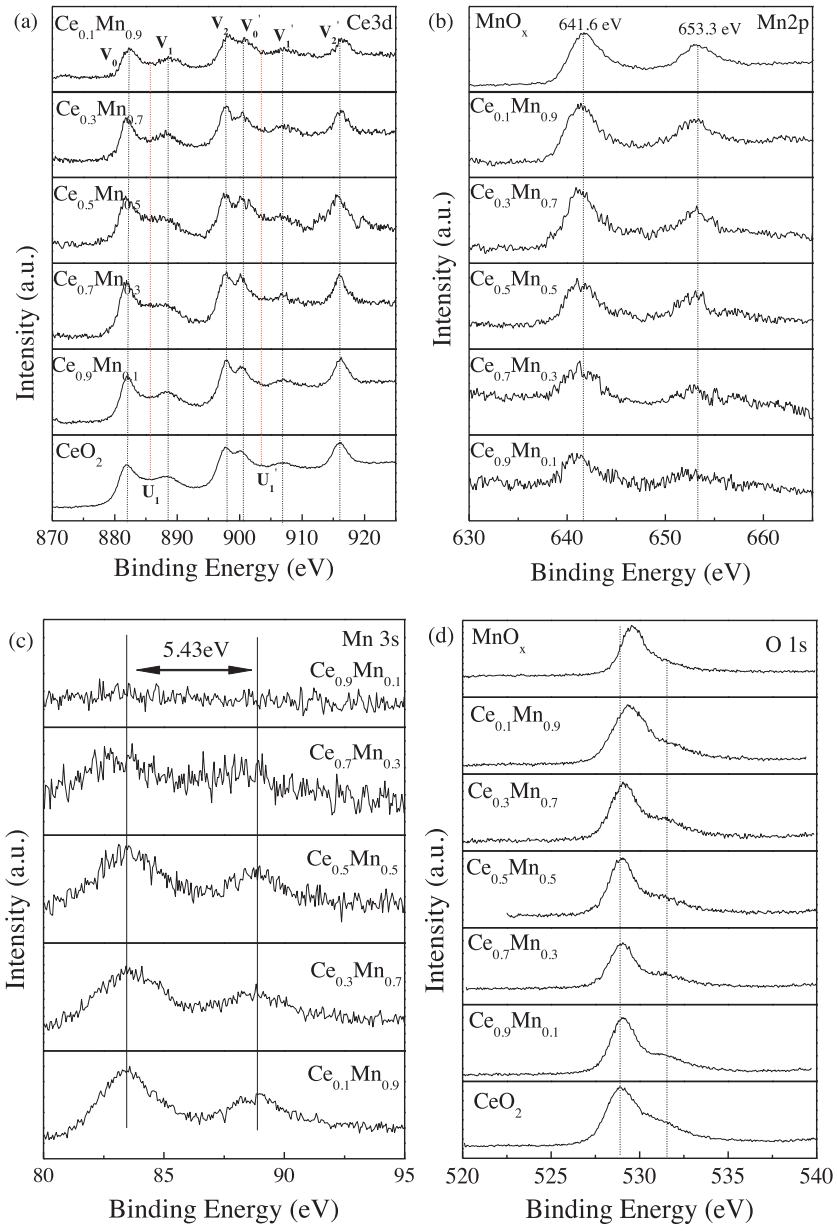

Fig. 4. X-ray photoelectron spectra in the Ce 3d (a), Mn 2p (b) and O 1s (c) regions for the Ce_xMn_{1-x} composite catalysts.

binding energy corresponds to Mn_2O_3. It should be noted, though, that the BEs of various Mn ions are very close to each other, rendering impossible the exact identification of oxidation states due to overlap of the energy ranges for various oxidation states of Mn [27,28]. However, the fact that the Mn 2p3/2 peak is rather broad may imply the co-existence of Mn^{2+} and Mn^{3+} ions at the surface of the catalysts. The XPS results do not provide any evidence for the presence of Mn^{4+} species (642.2–643 eV) [27,28]. In order to determine the chemical states of Mn further, Mn 3s XPS spectra of Ce_xMn_{1-x} are analyzed (Fig. 4c). The distance of the twin peaks in the spectra (ΔMn3s) is about 5.43 eV for all samples, closing to the value of 5.1 for the standard sample of α-Mn_2O_3. The ΔMn3s of MnO is about 6.3 eV, indicating that the oxidation status of Mn is predominantly tervalent [29,30]. In addition, the peak of Mn $2p_{3/2}$ (641.6 eV) for Ce_xMn_{1-x} composites is shifted to lower binding energy comparing with Mn_2O_3, which may be a consequence of interaction between CeO_2 and Mn_2O_3.

The XPS O1s spectra (Fig. 4d) show a main peak at a binding energy of 529.1–529.6 eV, corresponding to lattice oxygen of CeO_2 and MnO_x phases(O^{2-}; denoted as O_α) [22,27]. A broad shoulder at the higher binding energy region (531.5–532.7 eV) is ascribed to defective oxides or oxygen species of the surface carbonates and hydroxide (denoted as O_β) [20,31]. Table 1 shows the contents of O_α for Ce_xMn_{1-x} composites, CeO_2 and MnO_x. Obviously, the

Table 1
XPS results and Mn/Ce atomic ratio of Ce_xMn_{1-x} samples.

Sample	BE (eV)		$O_\alpha/(O_\alpha+O_\beta)$ (%)	Atomic ratio of Ce/Mn	
	O_α	O_β		ICP	XPS
CeO_2	529.0	531.3	80.21		
$Ce_{0.9}Mn_{0.1}$	529.0	531.2	83.28	8.22	10.88
$Ce_{0.7}Mn_{0.3}$	529.1	531.3	90.66	2.25	4.11
$Ce_{0.5}Mn_{0.5}$	529.1	531.3	90.78	1.03	1.41
$Ce_{0.3}Mn_{0.7}$	529.2	531.5	93.25	0.412	0.454
$Ce_{0.1}Mn_{0.9}$	529.3	531.5	91.14	0.12	0.29
MnO_x	529.6	531.6	83.26		

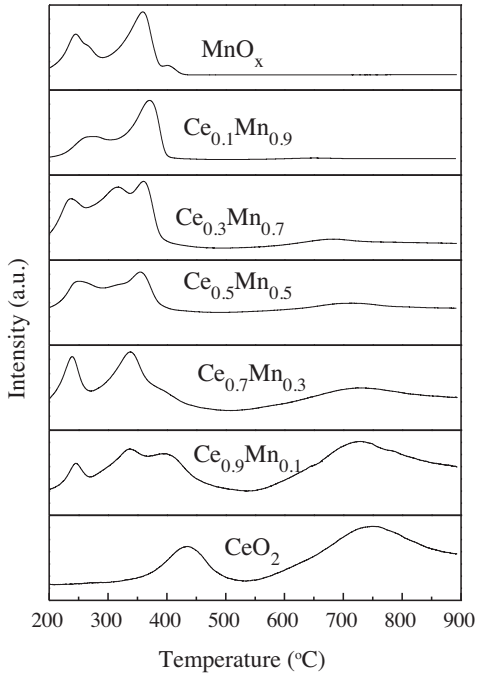

Fig. 5. H_2-TPR profiles of CeO_2, MnO_x and Ce_xMn_{1-x}.

$Ce_{0.3}Mn_{0.7}$ sample possesses more lattice oxygen species, confirming that the mobility and availability of lattice oxygen species are enhanced due to the synergistic effects of CeO_2 and MnO_x in $Ce_{0.3}Mn_{0.7}$ [32]. We deduce that O_α is the main active oxygen species and is responsible for the high catalytic activity of $Ce_{0.3}Mn_{0.7}$ in the complete oxidation of benzene. In addition, it is worthy to note that the peak corresponding to lattice oxygen in Ce_xMn_{1-x} composite catalyst with higher Mn content tends to shift toward higher BE value than that of pure CeO_2, which suggests that the environments of oxygen change with increasing Mn content.

To evaluate the dispersion of Mn ion at the catalyst surface and in bulk, the surface and bulk Mn/Ce atomic ratios (Mn 2P/Ce 3d) are calculated based on the XPS and ICP data, respectively. These results are also given in Table 1. For $Ce_{0.3}Mn_{0.7}$ and $Ce_{0.5}Mn_{0.5}$, the Ce/Mn surface value (0.454 and 1.41) is similar to the bulk atomic composition (0.412 and 1.03). This result demonstrates that MnO_x and CeO_2 are homogeneously dispersed in the $Ce_{0.3}Mn_{0.7}$ and $Ce_{0.5}Mn_{0.5}$ samples to form synergistic effect, which plays an important role in benzene catalytic oxidation. For $Ce_{0.9}Mn_{0.1}$, $Ce_{0.7}Mn_{0.3}$ and $Ce_{0.1}Mn_{0.9}$, the Ce/Mn surface values (10.88, 4.11 and 0.29) are larger than the bulk atomic composition (8.22, 2.25 and 0.12), which indicate that MnO_x and CeO_2 are not well dispersed in the composites. Their synergistic effect is weakened so that the catalytic abilities decrease.

In order to check the redox properties of the new series of Ce_xMn_{1-x} systems, TPR of all the catalysts were carried out. Fig. 5 shows the H_2-TPR profiles of CeO_2, MnO_x and Ce_xMn_{1-x} composite oxides. Similar to previous findings [33–35], pure CeO_2 exhibits two reduction peaks at around 435 °C and about 750 °C. The former low-temperature reduction is due to the removal of surface oxygen and the later high-temperature reduction is related to the oxygen species in bulk CeO_2. The H_2-TPR profile of pure MnO_x shows two strong reduction peaks at 245 and 360 °C, respectively, with an area ratio of the lower to the higher temperature hydrogen consumption of about 1:2. This is the typical feature of two-step reduction of Mn_2O_3, the low-temperature reduction peak represented the reduction of Mn_2O_3 to Mn_3O_4 and the high-temperature reduction peak referred to the further reduction of Mn_3O_4 to MnO [36]. This is in agreement with the XRD data, which show that the crystalline phase of pure MnO_x corresponds to Mn_2O_3.

Table 2
Position lifetime parameters of Ce_xMn_{1-x}, CeO_2 and MnO_x.

Sample	τ_1 (ps)	τ_2 (ps)	τ_3 (ns)	τ_{av} (ps)	I_1 (%)	I_2 (%)	I_3 (%)
CeO_2	204	400	5.4	348	39.06	60.45	0.49
$Ce_{0.7}Mn_{0.3}$	204	414	2.31	358	41.9	56.4	1.7
$Ce_{0.3}Mn_{0.7}$	202	415	3.30	325	42.2	57.4	0.4
MnO_x	179	424	2.20	322	51.2	47.5	1.3

In contrast to pure CeO_2 and MnO_x, the reduction profiles of Ce_xMn_{1-x} catalysts are more complicated. For $Ce_{0.9}Mn_{0.1}$, the reduction starts at ca. 200 °C and the TPR profile consists of three overlapping peaks at lower temperature and one peak at higher temperature. According to the reduction characteristics of pure MnO_x and CeO_2, it can be deduced that the lower temperature peaks (240 and 336 °C) are assigned to the two-step reduction of Mn_2O_3. The reduction of CeO_2 takes place concurrently along with reduction of manganese ions. The peak at 400 °C is corresponded to the reduction of surface oxygen in CeO_2 and the higher temperature peak (730 °C) is attributed to the oxygen species in bulk CeO_2. Meanwhile, it can be also realized that the reduction temperatures begin to drop and the peak corresponding to the oxygen species in bulk CeO_2 disappear gradually with the content of Mn increasing for other Ce_xMn_{1-x} composite oxides. This indicates that the reduction of the manganese oxide and the cerium oxide in the composite is promoted due to the formation of the solid solution (Mn—Ce—O), which facilitates the mobility of the oxygen species in the mixed oxide. Therefore, their catalytic activities over benzene are higher than pure CeO_2 and MnO_x.

It is worthy to note that the TPR profile of $Ce_{0.3}Mn_{0.7}$ exist obvious difference from those of other Ce_xMn_{1-x} composite oxides. Although the peaks attributed to the reduction of CeO_2 are also not found, three special peaks (ca. 240, 316 and 360 °C) over the temperature range (200–400 °C) are clearly detected. The peaks at 240 and 360 °C are still due to the reduction of Mn^{3+}, whereas the peak at 316 °C is possible to be caused by the synergistic effect between Mn^{3+} and Ce^{4+}, which results in the highest activity over benzene in the Ce_xMn_{1-x} composite oxides.

According to our past research [37], oxygen vacancies in the pure or doped CeO_2 play an important part in CO catalytic oxidation. In order to explain the mechanism of benzene catalytic oxidation further, we study the nature of defects in the Ce_xMn_{1-x} composite oxides. Positron annihilation spectrum is a well established technique to study defects in materials. The lifetime of the positron is able to give information about the size, type, and relative concentration of various defects/vacancies even at the ppm level. The positron lifetime spectra of the samples yielded three distinct lifetime components, τ_1, τ_2, and τ_3, with relative intensities I_1, I_2, and I_3 (Table 2). The longest component (τ_3) was due to the annihilation of orthopositronium atoms formed in the large voids present in the material [38,39]. The shortest one (τ_1) was attributed to small neutral Ce^{3+}-oxygen vacancy associates, probably in the form of $Ce'_{Ce}V_OCe'_{Ce}$ [40]. The oxygen vacancy is resulted from Mn ion replacing with Ce ion. Another component (τ_2), could be assigned to larger size defects clusters (dimmers, trimmers, or larger) in the materials, which are resulted from interaction between the small neutral Ce^{3+}-oxygen vacancy associates (τ_1) [39,41]. Besides the lifetime of the positron, its relative intensity (I) gave more information on the distribution of these defects since the relative intensity quantifies the abundance of that vacancy with respect to some standard of the same material [40]. Average lifetime (τ_{av}) can be used to

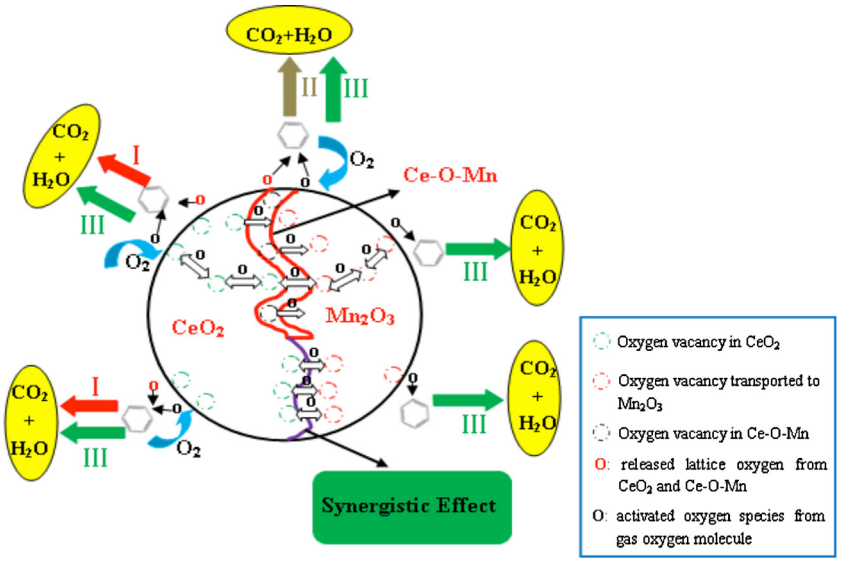

Fig. 6. The mechanism of benzene catalytic oxidation over Ce_xMn_{1-x} composite oxide.

character the overall situation of defects and calculated data are seen in Table 2.

$$\tau_{av} = \tau_1 I_1 + \tau_2 I_2 + \tau_3 I_3 \quad (2)$$

Through the table data, it can be acquired that the τ_{av} of $Ce_{0.7}Mn_{0.3}$ is longer that that of pure CeO_2 indicating that the concentration of oxygen vacancy increases due to Mn ion introduced into the crystal lattice of CeO_2, which is closely related with the higher catalytic activity of $Ce_{0.7}Mn_{0.3}$. Similar with signature referred above, the τ_{av} of $Ce_{0.3}Mn_{0.7}$ is longer that that of pure MnO_x, which shows that the concentration of oxygen vacancy is also enhanced due to Ce ion introduced into the crystal lattice of MnO_x, therefore, catalytic ability is enhanced. It is interesting to note that the τ_{av} of $Ce_{0.7}Mn_{0.3}$ is longer than that of $Ce_{0.3}Mn_{0.7}$, which indicate that the concentration of oxygen vacancy increases, however, the catalytic property is lower than that of $Ce_{0.3}Mn_{0.7}$ Therefore, it can be concluded that the oxygen vacancy is one of the key factors in determining catalytic property and synergistic effect between two phases may play more important part in benzene catalytic oxidation. The synergistic effect has also been indirectly identified by TEM, XPS and H_2-TPR data.

3.3. Mechanism discussion on benzene catalytic oxidation

According to the analysis above, the benzene catalytic oxidation mechanism for Ce_xMn_{1-x} is offered (Fig. 6). Benzene is oxidized by Ce_xMn_{1-x} oxides along three paths. In path (I), benzene that had been adsorbed on Ce_xMn_{1-x} oxides is oxidized by the release of oxygen from CeO_2 phase, because of storing oxygen capacity for cerium oxide; in path (II), benzene adsorbed on Ce_xMn_{1-x} oxides is oxidized by the release of oxygen from Ce_xMn_{1-x} oxides, due to the formation of Ce—O—Mn solid solution. In Ce—O—Mn solid solution, Ce^{4+} ion was substituted by Mn^{3+} ion to release lattice oxygen in order to balance charge; in path (III), benzene is oxidized by the active oxygen species from gas oxygen molecules, which are activated at the surface of catalyst to replenish the oxygen vacancies. Some activated oxygen directly oxidize the benzene at the surface of CeO_2 and Ce—O—Mn; and then other activated oxygen species are transported to the surface of Mn_2O_3 through oxygen vacancy (CeO_2 and Ce—O—Mn) and oxidize the benzene adsorbed on Mn_2O_3. It is worthy to note that the synergistic effect between CeO_2 and Mn_2O_3 can enhance the migration of oxygen vacancy to improve the catalytic activity. Therefore, the role of synergistic effect is important, even decisive in the whole catalytic process. The synergistic effect and oxygen vacancy are combined to promote the benzene oxidation mutually.

4. Conclusion

A series of Ce_xMn_{1-x} composite oxides, CeO_2 and MnO_x were synthesized through hydrothermal process under the same experimental condition. Their catalytic properties were studied comparatively through benzene oxidation. The results indicated that Ce_xMn_{1-x} catalysts exhibited better activities comparing with pure CeO_2 or MnO_x, among which the catalytic activity reached the best when the Ce_{at}/Mn_{at} optimum ratio was 3:7. The roles of crystal defects (oxygen vacancy) and synergistic effect were researched in benzene catalytic oxidation in detail. The data showed that the interaction between two phases was the determined factor.

Acknowledgements

The authors thank National Natural Science Foundation for the Youth of China (no. 51002037), Strategic pilot projects for science and technology of CAS (no. XDB05050000) and National 863 Program (no. 2010AA064903) for the support. The valuable discussion with Prof. Fabing Su is appreciated.

Appendix A. Supplementary data

Supplementary data associated with this article can be found, in the online version, at http://dx.doi.org/10.1016/j.apcatb.2013.02.030.

References

[1] H.S. Kim, T.W. Kim, H.L. Koh, S.H. Lee, B.R. Min, Applied Catalysis A: General 280 (2005) 125.
[2] K. Everaert, J. Baeyens, Journal of Hazardous Materials 109 (2004) 113.
[3] J.N. Armor, Applied Catalysis B: Environmental 1 (1992) 221.
[4] J.J. Spivey, Industrial and Engineering Chemistry Research 26 (1987) 2165.
[5] L.A. He, Y.B. Yu, C.B. Zhang, H. He, Journal of Environmental Science China 23 (2011) 160.
[6] L. Becker, H. Forster, Applied Catalysis B: Environmental 17 (1998) 43.
[7] R.S.G. Ferreira, P.G.P. de Oliveira, F.B. Noronha, Applied Catalysis B: Environmental 50 (2004) 243.
[8] J.J. Li, X.Y. Xu, Z. Jiang, Z.P. Hao, C. Hu, Environmental Science and Technology 39 (2005) 1319.

[9] T. Garcia, B. Solsona, D. Cazorla-Amoros, A. Linares-Solano, S.H. Taylor, Applied Catalysis B: Environmental 62 (2006) 66.
[10] M.F.M. Zwinkels, S.G. Jaras, P.G. Menon, T.A. Griffin, Catalysis Reviews – Science and Engineering 35 (1993) 319.
[11] C. Lahousse, A. Bernier, P. Grange, B. Delmon, P. Papaefthimiou, T. Ioannides, X. Verykios, Journal of Catalysis 178 (1998) 214.
[12] L. Lamaita, M.A. Peluso, J.E. Sambeth, H.J. Thomas, Applied Catalysis B: Environmental 61 (2005) 114.
[13] L. Lamaita, M.A. Peluso, J.E. Sambeth, H. Thomas, G. Mineli, P. Porta, Catalysis Today 107–108 (2005) 133.
[14] M.A. Peluso, E. Pronsato, J.E. Sambeth, H.J. Thomas, G. Busca, Applied Catalysis B: Environmental 78 (2008) 73.
[15] Q.G. Dai, X.Y. Wang, G.Z. Lu, Applied Catalysis B: Environmental 81 (2008) 192.
[16] H.J. Kim, S.W. Choi, H.I. Inyang, Environmental Technology 29 (2008) 559.
[17] S.M. Saqer, D.I. Kondarides, X.E. Verykios, Topics in Catalysis 52 (2009) 517.
[18] G.S. Qi, R.T. Yang, R. Chang, Applied Catalysis B: Environmental 51 (2004) 93.
[19] G.S. Qi, R.T. Yang, Journal of Catalysis 217 (2003) 434.
[20] X.F. Tang, Y.G. Li, X.M. Huang, Y.D. Xu, H.Q. Zhu, J.G. Wang, W.J. Shen, Applied Catalysis B: Environmental 62 (2006) 265.
[21] A.M.T. Silva, R.R.N. Marques, R.M. Quinta-Ferreira, Applied Catalysis B: Environmental 47 (2004) 269.
[22] M. Machida, M. Uto, D. Kurogi, T. Kijima, Chemistry of Materials 12 (2000) 3158.
[23] A. Pfau, K.D. Schierbaum, Surface Science 321 (1994) 71.
[24] W.D. Xiao, Q.L. Guo, E.G. Wang, Chemical Physics Letters 368 (2003) 527.
[25] F. Lenormand, L. Hilaire, K. Kili, G. Krill, G. Maire, Journal of Physical Chemistry 92 (1988) 2561.
[26] F. Larachi, J. Pierre, A. Adnot, A. Bernis, Applied Surface Science 195 (2002) 236.
[27] R. Dula, R. Janik, T. Machej, J. Stoch, R. Grabowski, E.M. Serwicka, Catalysis Today 119 (2007) 327.
[28] T. Rao, M.Q. Shen, L.W. Jia, J.J. Hao, J. Wang, Catalysis Communications 8 (2007) 1743.
[29] Y.F. Han, F. Chen, Z.Y. Zhong, K. Ramesh, L.W. Chen, E. Widjaja, Journal of Physical Chemistry B 110 (2006) 24450.
[30] Y. Luo, Y.Q. Deng, W. Mao, X.J. Yang, K. Zhu, J. Xu, Y.F. Han, Journal of Physical Chemistry C 116 (2012) 20975.
[31] H. Wang, H.Q. Zhu, Z.F. Qin, F.X. Liang, G.F. Wang, J.G. Wang, Journal of Catalysis 264 (2009) 154.
[32] Y.S. Wu, Y.X. Zhang, M. Liu, Z.C.C. Ma, Catalysis Today 153 (2010) 170.
[33] A. Trovarelli, Catalysis Reviews – Science and Engineering 38 (1996) 439.
[34] E. Aneggi, M. Boaro, C. de Leitenburg, G. Dolcetti, A. Trovarelli, Journal of Alloys and Compounds 408 (2006) 1096.
[35] Tana, M.L. Zhang, J. Li, H.J. Li, Y. Li, W.J. Shen, Catalysis Today 148 (2009) 179.
[36] X.F. Tang, J.L. Chen, Y.G. Li, Y. Li, Y.D. Xu, W.J. Shen, Chemical Engineering Journal 118 (2006) 119.
[37] Z. Wang, Q. Wang, Y.C. Liao, G.L. Shen, X.Z. Gong, N. Han, H.D. Liu, Y.F. Chen, ChemPhysChem 12 (2011) 2763.
[38] A. Sachdeva, S.V. Chavan, A. Goswami, A.K. Tyagi, P.K. Pujari, Journal of Solid State Chemistry 178 (2005) 2062.
[39] S. Dannefaer, T. Bretagnon, D. Kerr, Journal of Applied Physics 74 (1993) 884.
[40] X.W. Liu, K.B. Zhou, L. Wang, B.Y. Wang, Y.D. Li, Journal of the American Chemical Society 131 (2009) 3140.
[41] S. Dutta, S. Chattopadhyay, D. Jana, A. Banerjee, S. Manik, S.K. Pradhan, M. Sutradhar, A. Sarkar, Journal of Applied Physics 100 (2006) 114328.